Achieving rapid actuation in liquid crystal elastomers

Journal:	*National Science Open*
Manuscript ID	NSO20240013.R1
Manuscript Type:	Review
Date Submitted by the Author:	17-May-2024
Complete List of Authors:	Liu, Changyue; Tianmushan Laboratory; Beihang University, Materials Science and Engineering Jin, Liuchao; The Chinese University of Hong Kong, Mechanical and Automation Engineering Liao, Wei-Hsin; The Chinese University of Hong Kong, Mechanical and Automation Engineering; The Chinese University of Hong Kong, Institute of Intelligent Design and Manufacturing Wang, Zhijian; Tianmushan Laboratory; Beihang University, Materials Science and Engineering He, Qiguang; The Chinese University of Hong Kong, Mechanical and Automation Engineering
Keywords:	Liquid Crystal Elastomer, Soft Robotics, Rapid Actuation
Note: The following files were submitted by the author for peer review, but cannot be converted to PDF. You must view these files (e.g. movies) online.	
Figures.rar	

REVIEW

National Science Open
1: 2024xxxx, 2024
https://doi.org/10.1360/nso/xxxxxxxx

Materials Science

Special Topic: Flexible Electronic and Micro/Nanomanufacturing

Achieving rapid actuation in liquid crystal elastomers

Changyue Liu[1,2], Liuchao Jin[3], Wei-Hsin Liao[3], Zhijian Wang[1,2,*] and Qiguang He[3,*]

[1]*Tianmushan Laboratory, Hangzhou 310023, China;*
[2]*Key Laboratory of Aerospace Advanced Materials and Performance, Ministry of Education, School of Materials Science and Engineering, Beihang University, Beijing 100191, China;*
[3]*Department of Mechanical and Automation Engineering, The Chinese University of Hong Kong, Hong Kong, China*

*Corresponding authors (emails: zhijianw@buaa.edu.cn (Zhijian Wang); qiguanghe@cuhk.edu.hk (Qiguang He))

Received 23 April 2024; Revised 16 May 2024; Accepted 3 June 2024; Published online

Abstract: Liquid crystal elastomer (LCE) is one kind of soft actuating material capable of producing large and reversible actuation strain, versatile and programmable actuation modes, and high work density, which can be widely exploited for next-generation soft robots. However, the slow response speed and low power density in LCE-based actuators remain a challenge, limiting their practical applications. Researchers have been considering how to improve these performances. In this review, we discuss the fundamentals of the LCEs and emphasize the fast actuation strategies developed in recent years. Firstly, we introduce conventional preparation strategies. Then, we describe typical actuation mechanisms of LCEs, discussing their features and limitations. Subsequently, we summarize several possible approaches as case studies to enhance the actuation performance of LCEs, including reducing physical sizes, introducing active heating-cooling mechanisms, utilizing mechanical instability, and developing dielectric LCEs. Finally, we discuss the future research opportunities and challenges for rapid actuation of LCEs.

Keywords: liquid crystal elastomer, soft robotics, rapid actuation

INTRODUCTION

Robotics made from soft materials exhibit salient features, such as body compliance, large and continuous deformation, and benign human-machine interaction, which stand in contrast to their rigid counterparts [1]. These unique features make soft robots a promising candidate for broad applications in space exploration, rehabilitative devices, prostheses, and dexterous manipulations. In recent decades, numerous works have been dedicated to developing soft robots with various locomotion, grasping or manipulation, etc. For instance, Tolley *et al*. developed an untethered pneumatic soft quadruped that could crawl under extreme and harsh environments (e.g., snowstorms, water, and fire) [2]. Inspired by the characteristics of deep-sea creatures, Li *et al*. developed an untethered, self-powered soft robot that can be used for deep-sea exploration [3]. Practical tests were conducted at the deepest point of 10,900 m in the Mariana Trench. This soft robot exhibits exceptional pressure resistance and swimming performance owing to its electrostatic mechanism. Wood *et al*. presented an ultragentle soft robotic actuator that can grasp delicate specimens of gelatinous marine life. Three types of live jellyfish were successfully grasped and manipulated using the soft robotic gripper [4].

For all these examples, the soft actuating materials and deployable structures work as the “motor” to

drive the locomotion and conduct advanced functions. They are compliant and capable of producing large deformation in response to external stimuli. Recently, researchers have devoted lots of effort to developing various soft actuating materials with excellent performances [5], including dielectric elastomer actuators (DEAs), shape memory polymers (SMPs), hydrogels, magnetic soft materials (MSMs), and liquid crystal elastomers (LCEs). The DEA is a deformable capacitor made by sandwiching a dielectric elastomer (DE) film between two compliant electrodes. When subjected to voltage, DEAs generate a strong electrostatic interaction between two electrodes, compressing the film in the thickness direction and expanding it in the area (Figure 1A) [6,7]. The DEAs can produce rapid actuation when a large electric potential of several kilovolts is applied. However, high voltage conditions increase the complexity of the system and pose a potential safety threat to humans. SMPs can change morphology and stiffness when the temperature varies, owing to the phase transition or decrosslinking of temporary interaction (Figure 1B) [8,9]. Still, they usually have one-way actuation, which cannot recover to the initial shape after deformation. MSMs are made by dispersing magnetized or magnetizable microparticles in polymeric matrices (Figure 1C) [10,11]. These composites could deform wirelessly under an external magnetic field. It is fast and can be precisely controlled, which can be broadly used in biomedical applications. Nevertheless, the control of soft magnetic composites is limited by external magnetic fields. Responsive hydrogels, for example, poly(N-isopropylacrylamide) (PNIPAAm), can change into a hydrophobic state when the temperature is increased, leading to a volumetric shrinkage [12]. They have been widely studied in fields such as marine robots and biomedical tools (Figure 1D) [13,14]. However, the work mechanism of hydrogels relies on diffusion, causing a slow response speed.

[INSERT FIGURE 1 HERE]

Recently, LCEs have received significant interest due to their large reversible actuation strain, versatile and programmable actuation modes, and high work density. These distinctive characteristics make them an ideal option for achieving sensing and actuation functions in soft robots [15]. LCEs are a combination of liquid crystal mesogens and polymer networks, possessing anisotropy of mesogens and elasticity of polymer networks [16–18]. When subjected to external stimuli (e.g., temperature, light, non-polar solvents), LCEs undergo the nematic-isotropic phase transition, causing an anisotropic contraction (Figure 1E) [19–21]. By spatially patterning the mesogens, they can produce versatile in-plane or out-of-plane actuation modes, including bending, twisting, curling, and extension [22–24]. Once external stimuli are removed, LCEs fully recover to their initial shape, showing good reversibility. However, the actuation and recovery of the LCE are relatively slow compared to DEAs and conventional machines, significantly restricting their applications regardless of their large deformation, high work density, and easy actuating methods (Figure 2) [25–30]. Thus, it is emerging to develop strategies to produce rapid actuation in LCE materials.

[INSERT FIGURE 2 HERE]

In this review, we discuss the fundamentals of LCEs and highlight various strategies to improve their response speed and power density. First, we introduce different synthesis strategies for LCEs. Next, we present typical actuation methods of LCEs. Subsequently, four possible approaches to improve the response speed are highlighted, including reducing the critical length scale of LCEs, introducing active heating and cooling systems in LCEs, utilizing instability, and developing dielectric liquid crystal elastomers. Finally,

perspectives on challenges and opportunities for rapid actuation of LCEs are discussed.

SYNTHESIS AND ALIGNMENT OF LCES

The LCEs are made by integrating liquid crystal mesogens into a polymer network. The synthesis and processing of LCEs determine their actuation performance and application scenarios. The actuation behavior of LCEs is dependent on the anisotropic alignment of mesogens. Without additional treatment during preparation, the LCEs are usually in a polydomain state, in which the alignments of mesogens in different domains are random. Therefore, the polydomain LCEs cannot produce macroscopic deformation upon external stimuli. To achieve actuation capability, the mesogens should be highly aligned first and then fixed by a polymer network, namely monodomain LCEs. Several strategies have been explored in the past years to prepare the monodomain LCEs. They can be classified into three categories: one-step polymerization, two-step polymerization, and dynamic covalent network methods [31].

One-step polymerization method

In the one-step polymerization method, reactive liquid crystal molecules are used. When heated above the phase transition temperature, the small molecules have a low viscosity, which can be aligned by surface or external electric/magnetic field. Then, the aligned molecules are exposed to ultraviolet (UV) light or heat to form a polymer network, fixing the alignment of mesogens and producing the monodomain LCEs. The alignment patterns of the mesogens can be controlled through well-developed techniques, enabling versatile actuation modes and rich design space of LCEs. For instance, Zeng *et al*. prepared an LCE iris using photoalignment technology. The liquid crystal cell (20 μm thick) is constructed so that the mesogens adopt homeotropic alignment at the upper surface. In contrast, the bottom surface is coated with a photoalignment layer, resulting in radial alignment of the mesogens. Like the natural iris, the LCE can autonomously open and close in response to incident light intensity (Figure 3A) [32]. In another work, Yang *et al*. utilized a designed channel-pattern mold with a pattern feature size of 1 μm to prepare LCE films with programmable alignment [33]. 2D LCE films can be deformed upon thermal activation into desired 3D shapes, such as the complex human face.

In the surface alignment technique, the mesogen is usually aligned parallel to the surface, while the magnetic field can generate an alignment perpendicular to the substrate. For instance, Cui *et al*. utilized a pair of permanent magnets to prepare an LCE pillar micropattern, in which the mesogens are aligned along the pillar direction (Figure 3B) [34]. The pillar micropatterns can undergo reversible switching between adhesive and non-adhesive states in response to temperature changes. However, the thickness of the LCE film prepared by the surface alignment or magnetic/electric field-assisted alignment is limited to tens to hundreds of micrometers.

Two-step polymerization method

Unlike the one-step polymerization method, in the two-step polymerization method, the liquid crystal mesogens are first polymerized into linear oligomers or loosely crosslinked polymer networks with residual reactive groups inside. The mesogens are further aligned by mechanical force. Then, the alignment is fixed by forming a polymer network due to the crosslinking of residual reactive groups. The two-step polymerization method can be employed to prepare the LCE film on large scales. Finkelmann and coworkers first reported the two-step polymerization method for fabricating monodomain LCEs using two kinds of hydrosilylation reaction with different reaction rates [35]. Later, Yakacki *et al*. used a commercially

available liquid crystal mesogen that could undertake a two-stage thiol-acrylate Michael addition and photopolymerization reaction, significantly improving the simplicity and reproducibility of the monodomain LCEs (Figure 3C) [36].

In the two-step polymerization method, the mesogens can be first polymerized into linear oligomers, which are extrudable and thereby can be used as the ink in the direct ink writing (DIW) 3D printing technique, enabling the spatial alignment of mesogens by computer-aided design (CAD) [37–41]. In this way, LCEs can be fabricated in desired alignment patterns and shapes, thereby achieving customized deformation [42–44]. During the printing process, the mesogens are aligned along the printing direction via shear force and then are fixed by post-curing [45,46]. The degree of alignment can be tailored by printing parameters, such as the inner diameter of the nozzle, printing temperature, distance between the nozzle and substrate, etc. Wang *et al*. printed versatile active morphing structures with functionally graded LCEs by varying printing parameters, achieving the versatility of deformation and structure (Figure 3D) [47]. However, the spatial resolution of the alignment of mesogens is limited by the nozzle diameter (> 150 μm).

Dynamic covalent network method

The LCEs with regular covalent bonds prepared by one-step and two-step polymerizations are thermoset, and their actuation behavior cannot be reprogrammed, reprocessed, and recycled once cured. Ji *et al*. creatively introduced the dynamic covalent bonds (DCBs) into LCEs to make them reprogrammable and modulable (Figure 3E) [48]. The DCBs can undergo exchange reactions under external stimuli (such as heat or light), leading to the rearrangement of the polymer network. As a result, the LCE can be programmed into a monodomain state. The LCEs with DCBs exhibit reprocessing, reshaping, and self-healing abilities and can be assembled with modulable building blocks [49,50]. At present, numerous DCBs have been incorporated into LCEs, such as ester groups [51–56], disulfide bonds [57–59], boronic esters [60,61], Diels-Alder reactions [62], diselenide bonds [63], and so on.

[INSERT FIGURE 3 HERE]

ACTUATION METHODS OF LCES

The nematic-isotropic phase transition of LCEs can be triggered via thermal or photochemical stimuli, depending on the types of mesogens. Azobenzene derivatives are typical photo-responsive mesogens. They can undertake trans-cis transition upon applying ultraviolet light [64–66]. Ceamanos *et al*. showed that an LCE strip containing azobenzene could generate photochemical actuation (Figure 4A) [67]. After being irradiated by UV light, the azobenzene molecules undergo a transition from trans to cis isomer, and the LCE strip bends towards the light. After being exposed to blue light (455 nm) for 30 min or left in darkness for 24 hours, the LCE strip returns to its original shape. However, the depth of light penetration limits the photochemical actuation of LCEs. Compared with photochemical-responsive LCEs, thermally responsive LCEs have a variety of types and can be prepared from commercially available materials. When heated above the phase transition temperature (T_i), they could deform into desired shapes. Changing mesogens or tuning the crosslinking density can easily adjust the phase transition temperature. Regarding the activating approaches of the LCE, environmental heating, electrothermal, photothermal, and magnetothermal heating have been utilized to trigger the deformation by structural design. In the following, we introduce several recently developed heating actuation methods.

Environmental heating actuation

Environmental heating could directly induce the deformation of the whole structure. In this way, the LCE-based robots could exhibit locomotion or manipulation with the sequential on/off of environmental heating. Ji *et al*. made a tubular LCE gripper that can autonomously grab an object under a high-temperature environment. The object is released automatically when the gripper moves to a cold place [68]. In addition, environments with a gradient temperature field could also be employed to drive the autonomous motion of the LCE structures [69]. For instance, Cai *et al*. reported that a simple LCE rod could roll on a flat and hot surface, exhibiting the capability of environmental autonomy [70]. By modifying the structure of the LCE rod, Yin *et al*. subsequently developed a helical-shaped LCE with self-navigation capability. This robot can autonomously escape a complex maze (Figure 4B) [71,72]. Furthermore, Daraio *et al*. designed an assembled LCE pentagonal prism that can perform a programmed response to fold and roll when subjected to thermal stimuli [73]. Nevertheless, this design has been only used to produce limited rolling locomotion. By integrating thermally responsive cables, non-responsive cables, and stiff rods, Wang *et al*. constructed a self-propelling hybrid tensegrity structure that enables multimodal self-propelled motion [74]. For all these examples, the LCEs driven by environmental heat have relatively simple structures without the requirements of onboard control systems and power supplies (e.g., batteries).

Electrothermal actuation

Embedding electrothermal elements into the LCEs offers a significant convenience for actuation control and system integration. Once the voltage is applied, Joule heat can increase the temperature of LCEs and result in the actuation. The heating patterns and heating sequence/algorithm could be well designed and controlled to accomplish more efficient thermal regulation. Various heating elements have been embedded into LCE, including nanoparticles (e.g., graphite and silver paste) and metal wires (e.g., gold, copper, and liquid metal) [75–79]. The conductive nanoparticles are usually used as fillers and dispersed throughout the LCE precursors. While metallic wires are generally embedded into the LCEs as separate heaters through lamination or coaxial 3D printing, etc. For instance, Luo *et al*. demonstrated an electro-conductive LCE containing graphite/carbon black that produces 40% contraction under 150 V [80]. In parallel, stretchable electronics have also been integrated into LCE as heating elements and sensors. Yu *et al*. designed and fabricated ultrathin electronics innervated soft robots that can realize adaptable crawling locomotion through the conjugation of sensing and actuation [81]. Similar advanced functions have been demonstrated using liquid metal (LM) with high stretchability. Majidi and coworkers embedded LM micro droplets into the LCE matrix, forming an LM-LCE composite that can enhance thermal and electrical properties [82]. Additionally, LCE can be integrated via the 3D printing technique. Lewis *et al*. printed a core-shell LM-LCE fiber, which can be actuated by Joule heating and achieve closed-loop control based on changes in electric resistance [83]. Recently, Liu *et al*. created an LM-LCE actuator with programmable resistance regulated by gravity that exhibits a gravitropism response due to the dynamic interaction between the thermomechanical response of the actuator and the gravity [84]. Meanwhile, the electrical control methods provide a promising solution for making untethered soft robots at the system level. For example, He *et al*. created an untethered LCE robot by combining a lithium polymer battery, LCE tubular actuators, and a microcontroller, completely free from the restriction of an external power supply or control unit (Figure 4C) [85].

Photothermal actuation

The actuation of LCEs can also be stimulated via a photothermal mechanism. Compared to the photochemical mechanism, LCEs driven by the photothermal mechanism exhibit unique features, including

large penetration depth, long-term stability, and diverse materials selections. Multiple types of photothermal agents, including carbon nanotubes (CNTs) [86–88], gold nanorods (AuNRs) [89,90], polydopamine (PDA) [91,92], and MXene[93,94] have been incorporated into the LCE matrix. When LCEs are exposed to light, these doped agents directly transform light into heat, causing the temperature to increase and further induce the actuation. The photothermal actuation methods provide a remote control on the deformation of the actuators. For instance, Yang *et al*. designed a three-leaf panel folding structure prepared by CNT-LCE, which can generate jumping motion through energy storage and release (Figure 4D) [95]. Li *et al*. reported an MXene-LCE soft tubular actuator, which can exhibit adaptive phototropism and robust omnidirectional light-tracking capability in 3D space [96]. In addition to excellent photothermal conversion, MXene can be a sensor due to its high conductivity. Liu *et al*. produced a near-infrared-driven MXene-LCE bimorph membrane with self-sensing and feedback loop control functions. The microcontroller receives the signal of the resistance change and issues a command to modulate the near-infrared (NIR) laser irradiation to realize the closed-loop control of the LCE actuation [97]. Meanwhile, under a constant light source, light-driven LCEs can produce self-oscillation by a self-shadowing effect during photo-thermal-mechanical actuation and self-regulate by the resulting built-in negative feedback loop. He *et al*. developed a candle soot (CS)-doped LCE/polydimethylsiloxane (PDMS) bilayer structure that can achieve sunlight-powered self-oscillation [98].

Magnetothermal actuation

Magnetic nanoparticles, such as Fe_3O_4 nanoparticle [99,100], can also be introduced to endow LCEs with magnetothermal actuation. Under the alternating magnetic fields (AMFs), magnetic nanoparticles convert the energy of AMF into heat due to the hysteresis loss, relaxation processes and other factors, resulting in a temperature increase of LCEs [101]. The magnetothermal actuated LCEs can be controlled remotely in enclosed and confined spaces on account of the strong penetrating power of magnetic fields. Ji *et al*. developed a magnetothermal-responsive LCE actuator by dispersing Fe_3O_4 nanoparticles into LCE, which can exhibit different motion modes including large contraction (~ 80%), biaxial shrinkage, complex 3D patterns, and so on (Figure 4E) [102]. Furthermore, by integrating of LCEs with different contents of magnetic particles, local and sequential magnetic control has been achieved.

[INSERT FIGURE 4 HERE]

RAPID ACTUATION STRATEGIES FOR LCE ACTUATORS

As summarized above, the LCEs exhibit large deformation and high work density via different thermal activating methods. Nevertheless, the response times of LCEs, including the actuation and recovery, are limited to a few seconds. The slow response dramatically limits the practical applications of LCE actuators in soft robots. This is because the response of thermally driven LCEs depends on the thermal conductivity of the LCE materials and the heat diffusion process during the actuation.

Table 1 summarizes the actuation performance of conventional LCE-based soft actuators and human skeleton muscles [103]. It can be seen that the actuation strain, stress, and work density of LCEs are all comparable to human muscle. However, the response speed and power density are one magnitude lower than human muscle. Multiple strategies have been developed to address this challenge in recent years. These approaches include reducing critical size, introducing an active heating-cooling system, utilizing mechanical instability, and developing other actuation mechanisms. In this section, we will discuss these strategies in detail. Similar strategies can be applied to other thermally driven materials, such as shape memory polymers,

twisting nylon fibers, and hydrogels.

[INSERT TABLE 1 HERE]

Reducing the critical length scale of LCEs

The reversible actuation depends on the contraction and recovery speed of LCEs, which is determined by the thermal diffusion process. According to the thermal capacity model, the thermal time constant is determined by the equation: $\tau = \frac{d\rho c}{h}$, where d is the characteristic thickness of the LCE, ρ is the mass density, c is gravimetric specific heat capacity, and h is the convective coefficient. The LCE materials determine the density ρ, specific heat capacity c, and convective coefficient h. Therefore, reducing the critical length scale of LCEs shortens the thermal time constant, thereby significantly enhancing the response speed of LCEs. Moreover, the power density can also be improved since it is proportional to the frequency of actuators ($P \sim \sigma\varepsilon f$, where σ, ε and f are actuation stress, strain, and frequency, respectively.).

Fabricating LCE fibers by the spinning method

Researchers have used different manufacturing techniques to fabricate LCE fibers at the microscale [104,105]. The spinning method is widely adopted to convert liquid or solid precursor materials into continuous solid fibers with specific structures and properties. The commonly used methods to prepare LCE fibers include electrospinning, dry spinning, and multi-drawdown spinning techniques [106].

Electrospinning is a well-established method of producing microfibers by spraying and stretching polymer solution under electrostatic voltage [107,108]. For instance, using this technique, He *et al*. massively produced LCE microfiber actuators within a short period (Figure 5A) [109]. When a high voltage is applied between the LCE ink and the conductive target, the solvent is evaporated, and dry LCE fibers are obtained. These fibers can then be collected from the metallic target and exposed to UV light to undertake a cross-linking reaction. The diameters of LCE microfibers can be controlled in the range of 20 to 80 μm by adjusting spinning parameters, including ink concentration, voltage, and distance between the nozzle and collector. To precisely control the actuation in the micro-scale, the LCE fibers were coated with polydopamine (PDA). Based on the photothermal effect, it produced rapid actuation and recovery once the NIR was applied to the LCE. Quantitively, these LCE microfiber actuators exhibit large actuation strain (~ 60%), a fast response speed (< 0.2 s), and high power density (400 W kg^{-1}). These performances are all comparable to human skeleton muscle. Moreover, these LCE microfiber actuators can be used in multiscale robotic systems, such as micro tweezers, micro swimming robots, and light-power microfluidic impendent pumps. However, this work has two limitations. One is the non-uniformity of diameters of as-spun LCE fibers. Another challenge is that the mesogens of as-spun LCE microfibers are not aligned. Fibers always require external loads to align the mesogens along the axial direction, significantly limiting their practical uses.

In dry spinning technology, a spinning solution is extruded into hot air through a spinneret, causing the solvent to evaporate rapidly and the material to solidify into fibers [110]. Wei *et al*. fabricated PDA-modified MXene/LCE fibers via a dry spinning technology and a two-step cross-linking strategy (Figure 5B) [111]. The LCE microfibers designed possess uniform fiber diameter (710 ± 27 μm) and can generate large actuation strain (~ 60%) within 0.4 s. Furthermore, the LCE/MXene fibers can be further constructed as a smart circuit switch and a light-fueled adaptive photovoltaic smart window. The fibers produced by dry spinning are uniform, but their diameters are often large (hundreds of micrometers).

Inspired by the spiders who adopt unusual processes to produce fibers, Lv *et al*. developed a multi-

drawdown spinning technique that enables continuous and rapid production of aligned LCE fibers with uniform controllable diameters (Figure 5C) [112]. Through internal and external drawdowns and alignments, thin, aligned LCE fibers (the minimum diameter of 2.6 μm) can be successfully prepared. Both actuation stress and mechanical properties have been significantly enhanced by incorporating graphite. It is worth mentioning that LCE's actuation stress reaches 5.3 MPa, one magnitude higher than that of conventional LCE actuators and human muscle. As a result, the LCE fiber in this work exhibits high response frequency (50 Hz), unprecedented power density (20,440 W kg^{-1}), and remarkable durability (> 250,000 cycles without breakage). The multi-drawdown spinning technology possesses the unique capability that enables continuous and high-speed production of uniform thin microfibers with the well-defined orientation of mesogens, which few processing technologies can achieve.

Fabricating LCE fibers by extrusion method

LCE precursors are highly compatible with 3D printing processes, so extrusion methods, including direct ink writing (DIW) and melt electrowetting (MEW), have also been used to fabricate LCE fibers.

The DIW technology uses a nozzle to print a single filament that can be viewed as fiber [113–115]. Qi *et al*. developed a method for fabricating reversibly actuatable LCE fibers using DIW printing (Figure 5D) [116]. The obtained fibers have a modulus of 2 MPa, 51% actuation strain, and a failure strain of well over 100%. Yang *et al*. subsequently coated LM on the LCE fibers prepared by DIW printing, achieving a programmable electrothermal actuation response [117]. Applying pulsed voltage electrical stimulation allows LM-LCE fibers to contract at a maximum rate of 284 % s^{-1} and produce a large contraction ratio of over 40%. Furthermore, the LM-LCE fibers exhibit high power density (367 W kg^{-1}) and work density (417 kJ m^{-3}).

Fiber diameters in hundreds of microns are typically achieved via DIW. On the other hand, the MEW method integrates principles from melt electrospinning (MES) with extrusion-based 3D printing technologies to accurately place ultrafine fibers and fabricate intricate polymer microstructures [118,119]. Somolinos *et al*., for the first time, reported the successful electrowetting of photopolymerizable liquid crystal inks leading to LCE fibers with diameters ranging from several hundred nanometers to tens of microns [120]. In addition, complex fiber-based scaffolds with programmable and reversible deformation can be fabricated. In another work, using the MEW method, Wang and coworkers fabricated LCE-based microfiber actuators and various 3D actuators on the micrometer to centimeter scales with high resolutions (4.5 to 60 μm), actuation strains (10 to 55%) and a maximum work density of 160 J kg^{-1}. Moreover, based on a deep learning model, large-scale, real-time, LCE grid-based spatial temperature field sensors were designed, exhibiting a fast response time (< 42 ms) and a high precision (94.79%) (Figure 5E) [121].

Fabricating ultrathin LCE films

In addition to LCE fiber, ultrathin LCE films exhibit fast actuation and high power density with a small thermal inertia. Wang *et al*. developed a compression-assisted mold-casting method to fabricate ultrathin LCE film (Figure 5F) [122]. The compressive loads can quantitively control the thickness of the film. For instance, the minimal thickness of the LCE film can reach 10 μm under a load of 100 N. A thin layer of gold was sputtered on the LCE film as a heating element to trigger the actuation via an electro-thermal mechanism. Subject to a voltage pulse, LCE thin film instantaneously contracts with remarkable 750 % s^{-1} strain rates and 1,360 W kg^{-1} power density, several times beyond the human skeleton and insect flight muscles. Moreover, due to their electrical controlling method, the LCE thin films can be used as motor units and directly integrated into multiple dexterous artificial neuromuscular systems for rapid manipulation and

closed-loop control. However, the ultrathin LCE films sacrifice the magnitude of the actuation force due to the small area of cross section. It can be improved by the assembly of multiple films.

[INSERT FIGURE 5 HERE]

The size reduction of LCEs significantly improves the response speed and power density. However, the output force of the LCE actuator will also be diminished. It is emerging to address this challenge for further exploration. One feasible solution is to have an assembly that arranges multiple fibers (or thin films) in parallel, forming a bundle. However, the distance between individual actuators is critical since it significantly affects the thermal process, which requires careful design.

Introducing active heating and cooling systems in LCEs

Conventional LCE-based actuators rely on passive cooling to reduce the temperature for recovery. The response time depends on the critical length of the specimen. As a result, the cooling time scale is several seconds with a thickness of millimeters, which is relatively slow. According to thermal diffusion, $\tau = \frac{d^2}{\alpha}$, the thermal time constant is proportional to the square of the characteristic length of LCE d, and inversely proportional to thermal diffusivity α (constant for LCE). Therefore, reducing the characteristic length of LCE shortens the response time. Researchers have introduced microfluidic channels to realize an active cooling method in LCE actuators with large scale (~mm). In this way, low-temperature fluids could internally and actively flow through microfluidic channels to accelerate the cooling process of LCE. He *et al*. developed a fluid-driven LCE actuator comprising two layers of LCE film and a middle layer patterned with a fluidic channel [123]. By injecting hot water (95°C) into its internal fluidic channel, the LCE actuator could contract by 40% of its initial length within 10 s. Adopting active cooling methods to reduce the temperature of the LCE actuator, cold water (23°C) is injected into the internal fluidic channel, and the LCE actuator recovers to its initial length of about 10 s, which is much faster than external and passive air cooling. However, the delamination between layers caused by weak bonding usually happens under cyclic actuation, resulting in the leakage and failure of the actuator.

The development of LCE materials offers a new opportunity to address the bonding issue. Recent work has shown that LCE with dynamic disulfide covalent bonds possess self-healing, re-processing, and recycling capabilities. A disulfide exchange reaction occurs by heating above the reactive temperature, which could firmly bond all three layers (two thin film layers and a fluidic channel layer). As a result, the LCE actuator containing disulfide bonds can sustain the fluids with high temperatures and large flow rates without any leakages. In Figure 6A, by alternatively injecting hot (90°C) and cold water (20°C) into its internal fluid channel, it generates fast actuation as well as recovery [124]. The temperature and flow rates of the fluids regulate the actuation strain (~30%), stress (~0.3 MPa), and frequency (~1 Hz) of LCE actuators. Using the same principle, a bi-morph actuator-based soft gripper was further developed to handle objects with different features. The internal active heating and cooling system offers another opportunity for LCE to be operated in a broad range of temperatures. In a high-temperature environment, the LCE spontaneously deforms based on its phase transition. Through actively injecting cold water into its internal fluidic channel, a temperature gradient will be generated, resulting in the actuation of LCE. However, the fluid regulations require multiple mechatronics, including microcontrollers, pumps, solenoid valves, and circuits. These components are quite complex and bulky, which limits the untethered actuation of LCE.

Thermoelectric devices realize the mutual conversion between thermal and electrical energy based on Peltier effects. As an electrical current passes through the devices, heat is absorbed or released at the joints of

conductors, depending on the flow direction of the current. Using this principle, Majidi *et al*. embedded a soft, stretchable thermoelectric device (TED) into LCE, realizing active cooling driven by the voltages (Figure 6B) [125]. Specifically, when a current is applied to TED, a temperature gradient will be generated via the Peltier effect that causes the local contraction of LCE, resulting in the bending of the LCE in a specific direction (e.g., counterclockwise). Reversing the current flow cause the LCE to bend in the opposite direction (e.g., clockwise). The applied voltages determined the magnitude of bending angles and angular velocity of LCE. The maximum bending angle of 27° and angular velocity of 2.5 ° s^{-1} can be achieved under the voltage of 2.9 V. Compared to conventional LCE bending actuators of the same size, TED-LCE is one order of magnitude faster due to its unique internal and active cooling approach. Additionally, TED provides more advanced functions, such as energy-harvesting capability.

[INSERT FIGURE 6 HERE]

Utilizing mechanical instability

Mechanical instability has recently been applied to diverse actuating materials for fast motion using different design principles [126]. In nature, biological structures and organisms instantaneously release their stored energy using mechanical instabilities to produce high-speed locomotion, fast grasping, and shape reconfiguration. It has also been utilized to tackle the actuation speed of LCE actuators.

White *et al*. introduced snap-through instability into LCEs, achieving rapid jumping locomotion (Figure 7A) [127]. The LCEs with spatial variation of the nematic director of +1 topological defects were prepared, which can deform into a cone during heating. Two LCE films with different moduli were prepared by adjusting the crosslinking density. They laminated two soft LCE films with lower modulus and one stiff LCE film with higher modulus, ensuring that defect centers and edges of the squares were aligned to obtain an LCE device with the required modulus gradient. When the LCE device was placed on a hot surface (160°C) with the high modulus side downwards, only the bottom high modulus surface was initially heated and underwent strain. The film first deformed upwards into a cone, thereby storing elastic energy. Subsequently, due to the larger deformation on the lower modulus side of the upper layer, the curvature of the LCE film was reversed through mechanical instability, resulting in a snap-through instability in the center of the device, forming an inverted cone. The LCE device underwent rapid jumping due to this snap-through deformation, converting the stored elastic energy into kinetic energy. The force and acceleration of this transition caused the LCE to jump from the surface in less than 6 ms, reaching a height over 200 times the material thickness and 2.5 times the width of the LCE device.

Wie *et al*. reported a continuous photomechanical jumping of azobenzene-liquid crystal polymer network (LCN) monolith with on-demand height and angle programmability (Figure 7B) [128]. The LCN monoliths are designed as the spring-like 270° super twisted nematic (STN) molecular architecture to impart macroscopic bi-stability reliably. The perpendicular molecular alignment at the top and bottom of the LCN monoliths provides for the effective accumulation of photogenerated stress from the modified energy barrier between nonisometric structures, realizing jumping by instantaneously releasing energy via snap-through. Remarkably, the maximum jumping height reaches 15.5 body length (BL) with a maximum instantaneous velocity of 880 BL s^{-1}. By varying macroscopic geometry (the aspect ratio) and light intensity profile, the jumping height and angle of the LCN monoliths can be programmed. Furthermore, by selective switching of the light irradiation direction according to the post-landing film curvature, continuous jumping motions can be reliably implemented with a single LCN monolith. Four continuous and directional jumping sequences are demonstrated within 5 s to overcome an obstacle. The LCE actuators based on mechanical instability for

rapid actuation typically generate jumping locomotion, achieving more generalized behaviors in LCEs remains a challenge.

[INSERT FIGURE 7 HERE]

Developing dielectric liquid crystal elastomers

Dielectric elastomer actuators (DEAs) have been widely discovered due to their large actuation strain, fast response, high energy efficiency, and energy density. Multiple materials and structures have been used as DEAs, including 3M VHB tape, polydimethylsiloxane (PDMS), and hydraulically amplified self-healing electrostatic (HASEL). When subjected to high voltage (> 5 kV), a compressive Maxwell stress will be produced along the thickness direction, causing a rapid expansion of DE-film in the other two directions. Recently, an electro-mechanical actuation mechanism of dielectric liquid crystal elastomers (DLCEs) has been developed that combines the desirable characteristics of both DEAs and LCEs, exhibiting fast and highly efficient actuation and shape programmability.

Cai *et al*. developed a novel DLCE actuator that relatively low voltages could drive compared with traditional DEAs (Figure 8A) [129]. The soft elasticity and the pre-stretch ratio of DLCEs produced the desirable stress-strain relation in terms of low modulus, early strain-stiffening, and high dielectric permittivity. These properties enable the DLCEs to generate large actuation strain (~40%) at 1 Hz under a low voltage of 300 V. Additionally, the electromechanical actuation mechanism results in higher energy conversion efficiency (20%) than thermally-driven LCEs (< 1%). Moreover, versatile rapid actuation modes can be achieved by spatially programming the alignment of mesogens and local cross-linking density of DLCE. For instance, White *et al*. demonstrated a three-dimensional cone deformation of DLCE under Maxwell stress (Figure 8B) [130]. In this example, the orientation of mesogens in DLCE is in a circumferential direction. The material is soft in the radial direction but stiff along the circumferential direction. Therefore, this DLCE expands radially upon applying electrical potential, resulting in a 3D cone shape. In another work, Yang *et al*. also demonstrated programmable 2D to 3D shape changes (e.g., nonlocal Gaussian curvature) with large actuation strain (> 1,800%) and fast response time (~1 s) (Figure 8C) [131]. Recently, Xie *et al*. reported a low e-field (8 V μm^{-1}) driven multimodal DLCE actuator (Figure 8D) [132]. Specifically, the temporary and permanent shapes through the LC phase transition possess different bending stiffness, which leads to distinct actuation modes under an electric field, achieving mode-switching upon temperature change. Moreover, the temporary and permanent shapes can be reprogrammed so the multimodal actuation can be further diversified on demand. Regarding practical applications, various DLCE-based devices have been developed recently, including artificial muscles, tunable smart lenses, and haptic devices. DLCEs can achieve rapid actuation while requiring high input voltage due to the limitation in electrostatic mechanisms.

[INSERT FIGURE 8 HERE]

CONCLUSION AND OUTLOOK

Figure 9 compares the fast-actuated LCE with conventional LCE actuators regarding frequency and power density. Adopting the abovementioned four strategies has greatly enhanced the response speed and power density by two orders of magnitude, comparable to human skeleton muscle. The response frequency of the fast actuated LCEs can reach 1 Hz or even higher. Despite significant progress in fast-actuated LCEs, several challenges still exist.

[INSERT FIGURE 9 HERE]

Although the actuation performance has been enhanced, one-dimensional LCE microfibers produce limited output force. To magnify this force, multiple fibers have to be arranged in parallel to form a fiber bundle. However, the distance between individual fibers is critical as it greatly affects heat transfer. Additionally, LCE microfiber and ultrathin film can only generate contractile actuation once triggered. Converting 1D or 2D LCE in-plane contraction into diverse three-dimensional deformation is challenging. As demonstrated in previous work, one possible way is to combine LCE fiber with fabrics to induce complex 3D deformation [133,134]. For the 2D film, a feasible approach is to program the arrangement of mesogens leveraging advanced manufacturing techniques (e.g., two-photon polymerization). Moreover, the regulation of the fluids requires external control systems. It still faces challenges in constructing an untethered robotic system for locomotion and manipulation. Furthermore, the LCE actuators based on mechanical instability for rapid actuation typically generate jumping locomotion, achieving broader actuation in LCE remains a challenge. Lastly, DLCEs have to be activated by high voltage inputs, which requires the voltage amplifier and associated circuits to achieve.

The design of high-performance LCE actuators is a multidisciplinary subject that blends knowledge across various fields, including materials science, applied mechanics, additive manufacturing, and robotics. We hope our review could inspire soft robotics design and novel devices using LCEs.

Data availability

All data needed to evaluate the conclusions in the paper are present in the paper.

Funding

This work was supported by the National Key Research and Development Program of China (2023YFB3812500), the "Pioneer" and "Leading Goose" R&D Program of Zhejiang (2024SSYS0082), the National Natural Science Foundation of China (52105003), the Beijing Municipal Natural Science Foundation (2222058), the CUHK academic equipment funding under grant 4937214, and CUHK Direct Grant 4055217.

Conflict of interest

The authors declare that they have no conflict of interest.

References

1 Wehner M, Truby RL, Fitzgerald DJ, *et al.* An integrated design and fabrication strategy for entirely soft, autonomous robots. *Nature* 2016; **536**: 451–455.

2 Tolley MT, Shepherd RF, Mosadegh B, *et al.* A resilient, untethered soft robot. *Soft Robot* 2014; **1**: 213–223.

3 Li G, Chen X, Zhou F, *et al.* Self-powered soft robot in the Mariana Trench. *Nature* 2021; **591**: 66–71.

4 Sinatra NR, Teeple CB, Vogt DM, *et al.* Ultragentle manipulation of delicate structures using a soft robotic gripper. *Sci Robot* 2019; **4**: eaax5425.

5 Li M, Pal A, Aghakhani A, *et al.* Soft actuators for real-world applications. *Nat Rev Mater* 2022; **7**: 235–249.

6 Pelrine R, Kornbluh R, Kofod G. High-strain actuator materials based on dielectric elastomers. *Adv Mater* 2000; **12**: 1223–1225.

7 Shi Y, Askounis E, Plamthottam R, *et al.* A processable, high-performance dielectric elastomer and multilayering process.

Science 2022; **377**: 228–232.
8 Xie T. Tunable polymer multi-shape memory effect. *Nature* 2010; **464**: 267–270.
9 Luo L, Zhang F, Wang L, *et al.* Recent advances in shape memory polymers: multifunctional materials, multiscale structures, and applications. *Adv Funct Mater* 2023; **34**: 2312036.
10 Kim Y, Yuk H, Zhao R, *et al.* Printing ferromagnetic domains for untethered fast-transforming soft materials. *Nature* 2018; **558**: 274–279.
11 Kim Y, Parada GA, Liu S, *et al.* Ferromagnetic soft continuum robots. *Sci Robot* 2019; **4**: eaax7329.
12 Zhao Y, Xuan C, Qian X, *et al.* Soft phototactic swimmer based on self-sustained hydrogel oscillator. *Sci Robot* 2019; **4**: eaax7112.
13 Qian X, Zhao Y, Alsaid Y, *et al.* Artificial phototropism for omnidirectional tracking and harvesting of light. *Nat Nanotechnol* 2019; **14**: 1048–1055.
14 Lo C, Zhao Y, Kim C, *et al.* Highly stretchable self-sensing actuator based on conductive photothermally-responsive hydrogel. *Mater Today* 2021; **50**: 35–43.
15 He Q, Yin R, Hua Y, *et al.* A modular strategy for distributed, embodied control of electronics-free soft robots. *Sci Adv* 2023; **9**: eade9247.
16 Ohm C, Brehmer M, Zentel R. Liquid crystalline elastomers as actuators and sensors. *Adv Mater* 2010; **22**: 3366–3387.
17 Herbert KM, Fowler HE, McCracken JM, *et al.* Synthesis and alignment of liquid crystalline elastomers. *Nat Rev Mater* 2022; **7**: 23–38.
18 Mistry D, Traugutt NA, Yu K, *et al.* Processing and reprocessing liquid crystal elastomer actuators. *J Appl Phys* 2021; **129**: 130901.
19 Maurin V, Chang Y, Ze Q, *et al.* Liquid crystal elastomer-liquid metal composite: ultrafast, untethered, and programmable actuation by induction heating. *Adv Mater* 2023; **36**: 2302765.
20 Lan R, Shen W, Yao W, *et al.* Bioinspired humidity-responsive liquid crystalline materials: from adaptive soft actuators to visualized sensors and detectors. *Mater Horiz* 2023; **10**: 2824–2844.
21 McBride MK, Martinez AM, Cox L, *et al.* A readily programmable, fully reversible shape-switching material. *Sci Adv* 2018; **4**: eaat4634.
22 White TJ, Broer DJ. Programmable and adaptive mechanics with liquid crystal polymer networks and elastomers. *Nat Mater* 2015; **14**: 1087–1098.
23 Xiao Y, Wu J, Zhang Y. Recent advances in the design, fabrication, actuation mechanisms and applications of liquid crystal elastomers. *Soft Science* 2023; **3**: 11.
24 Nie ZZ, Wang M, Yang H. Structure-induced Intelligence of Liquid Crystal Elastomers. *Chem Eur J* 2023; **29**: e202301027.
25 Rich SI, Wood RJ, Majidi C. Untethered soft robotics. *Nat Electron* 2018; **1**: 102–112.
26 Zhai Y, Wang Z, Kwon KS *et al.* Printing multi-material organic haptic actuators. *Adv Mater* 2021; **33**: 2002541.
27 Won P, Kim KK, Kim H *et al.* Transparent soft actuators/sensors and camouflage skins for imperceptible soft robotics. *Adv Mater* 2021; **33**: 2002397.
28 Pang W, Xu S, Liu L *et al.* Thin-film-shaped flexible actuators. *Adv Intell Syst* 2023; **5**: 2300060.
29 Qu J, Xu Y, Li Z *et al.* Recent advances on underwater soft robots. *Adv Intell Syst* 2024; **6**: 2300299.
30 Leanza S, Wu S, Sun X *et al.* Active materials for functional origami. *Adv Mater* 2024; **36**: 2302066.
31 Wang Z, Cai S. Recent progress in dynamic covalent chemistries for liquid crystal elastomers. *J Mater Chem B* 2020; **8**: 6610–6623.
32 Zeng H, Wani OM, Wasylczyk P, *et al.* Self-regulating iris based on light-actuated liquid crystal elastomer. *Adv Mater* 2017; **29**: 1701814.
33 Aharoni H, Xia Y, Zhang X, *et al.* Universal inverse design of surfaces with thin nematic elastomer sheets. *P Natl Acad Sci* 2018; **115**: 7206–7211.
34 Cui J, Drotlef DM, Larraza I, *et al.* Bioinspired actuated adhesive patterns of liquid crystalline elastomers. *Adv Mater* 2012; **24**: 4601–4604.
35 Küpfer J, Finkelmann H. Nematic liquid single crystal elastomers. *Makromol Chem Rapid Commun* 1991; **12**: 717–726.
36 Yakacki CM, Saed M, Nair DP, *et al.* Tailorable and programmable liquid-crystalline elastomers using a two-stage thiol-acrylate reaction. *RSC Adv* 2015; **5**:18997–19001.

37 Wang Z, Guo Y, Cai S, *et al.* Three-dimensional printing of liquid crystal elastomers and their applications. *ACS Appl Polym Mater* 2022; **4**: 3153–3168.

38 Chen M, Hou Y, An R, *et al.* 4D Printing of reprogrammable liquid crystal elastomers with synergistic photochromism and photoactuation. *Adv Mater* 2023; **36**: 2303969.

39 Mistry D, Traugutt NA, Sanborn B, *et al.* Soft elasticity optimises dissipation in 3D-printed liquid crystal elastomers. *Nat Commun* 2021; **12**: 6677.

40 Kotikian A, Truby RL, Boley JW, *et al.* 3D printing of liquid crystal elastomeric actuators with spatially programed nematic order. *Adv Mater* 2018; **30**: 1706164.

41 Kotikian A, Watkins AA, Bordiga G, *et al.* Liquid crystal elastomer lattices with thermally programmable deformation via multi-material 3D printing. *Adv Mater* 2024; **36:** 2310743.

42 Saed MO, Ambulo CP, Kim H, *et al.* Molecularly-engineered, 4D-printed liquid crystal elastomer actuators. *Adv Funct Mater* 2019; **29**: 1806412.

43 Wang Y, Guan Q, Lei D, *et al.* Meniscus-climbing system inspired 3D printed fully soft robotics with highly flexible three-dimensional locomotion at the liquid-air interface. *ACS Nano* 2022; **16**: 19393–19402.

44 Wang Y, Yin R, Jin L, *et al.* 3D-printed photoresponsive liquid crystal elastomer composites for free-form actuation. *Adv Funct Mater* 2023; **33**: 2210614.

45 Sun Y, Wang L, Zhu Z, *et al.* A 3D-printed ferromagnetic liquid crystal elastomer with programmed dual-anisotropy and multi-responsiveness. *Adv Mater* 2023; **35**: 2302824.

46 Chen M, Gao M, Bai L, *et al.* Recent advances in 4D printing of liquid crystal elastomers. *Adv Mater* 2023; **35**: 2209566.

47 Wang Z, Wang Z, Zheng Y, *et al.* Three-dimensional printing of functionally graded liquid crystal elastomer. *Sci Adv* 2020; **6**: eabc0034.

48 Pei Z, Yang Y, Chen Q, *et al.* Mouldable liquid-crystalline elastomer actuators with exchangeable covalent bonds. *Nat Mater* 2014; **13**: 36–41.

49 Saed MO, Gablier A, Terentjev EM. Exchangeable Liquid Crystalline Elastomers and Their Applications. *Chem Rev* 2022; **122**: 4927–4945.

50 Zhu Y, Xu Z, Wu F, *et al.* Liquid-crystal elastomers based on covalent adaptable networks: From molecular design to applications. *Sci China Mater* 2023; **66**: 3004–3021.

51 Yang Y, Terentjev EM, Zhang Y, *et al.* Reprocessable thermoset soft actuators. *Angew Chem Int Ed* 2019; **58**: 17474–17479.

52 Yao Y, He E, Xu H, *et al.* Enabling liquid crystal elastomers with tunable actuation temperature. *Nat Commun* 2023; **14**: 3518.

53 Liu Y, Wu Y, Liang H, *et al.* Rewritable Electrically Controllable Liquid Crystal Actuators. *Adv Funct Mater* 2023; **33**: 2302110.

54 Liang H, Zhang S, Liu Y, *et al.* Merging the Interfaces of different shape-shifting polymers using hybrid exchange reactions. *Adv Mater* 2023; **35**: 2202462.

55 Pei Z, Yang Y, Chen Q, *et al.* Regional shape control of strategically assembled multishape memory vitrimers. *Adv Mater* 2016; **28**: 156–160.

56 Yao Y, He E, Xu H, *et al.* Fabricating liquid crystal vitrimer actuators far below the normal processing temperature. *Mater Horiz* 2023; **10**: 1795–1805.

57 Wang Z, He Q, Wang Y, *et al.* Programmable actuation of liquid crystal elastomers via "living" exchange reaction. *Soft Matter* 2019; **15**: 2811–2816.

58 Wang Z, Tian H, He Q, *et al.* Reprogrammable, reprocessible, and self-healable liquid crystal elastomer with exchangeable disulfide bonds. *ACS Appl Mater Interfaces* 2017; **9**: 33119–33128.

59 Wang Y, Wang Z, He Q, *et al.* Electrically controlled soft actuators with multiple and reprogrammable actuation modes. *Adv Intell Syst* 2020; **2**: 1900177.

60 Saed MO, Gablier A, Terentejv EM. Liquid crystalline vitrimers with full or partial boronic-ester bond exchange. *Adv Funct Mater* 2020; **30**: 1906458.

61 Ma J, Yang Y, Valenzuela C, *et al.* Mechanochromic, shape-programmable and self-healable cholesteric liquid crystal elastomers enabled by dynamic covalent boronic ester bonds. *Angew Chem Int Ed* 2022; **61**: e202116219.

62 Jiang ZC, Xiao YY, Yin L, *et al.* "Self-lockable" liquid crystalline diels-alder dynamic network actuators with room

temperature programmability and solution reprocessability. *Angew Chem Int Ed* 2020; **59**: 4925–4931.

63 Chen L, Bisoyi HK, Huang Y, *et al.* Healable and rearrangeable networks of liquid crystal elastomers enabled by diselenide bonds. *Angew Chem Int Ed* 2021; **60**: 16394–16398.

64 Lv J, Wang W, Xu J, *et al.* Photoinduced bending behavior of cross-linked azobenzene liquid-crystalline polymer films with a poly(oxyethylene) backbone. *Macromol Rapid Commun* 2014; **35**: 1266–1272.

65 Wani OM, Zeng H, Priimagi A. A light-driven artificial flytrap. *Nat Commun* 2017; **8**: 15546.

66 Gelebart AH, Jan Mulder D, Varga M, *et al.* Making waves in a photoactive polymer film. *Nature* 2017; **546**: 632–636.

67 Ceamanos L, Kahveci Z, López-Valdeolivas M, *et al.* Four-dimensional printed liquid crystalline elastomer actuators with fast photoinduced mechanical response toward light-driven robotic functions. *ACS Appl Mater Interfaces* 2020; **12**: 44195–44204.

68 Qian X, Chen Q, Yang Y, *et al.* Untethered recyclable tubular actuators with versatile locomotion for soft continuum robots. *Adv Mater* 2018; **30**: 1801103.

69 Feng W, He Q, Zhang L. Embedded physical intelligence in liquid crystalline polymer actuators and robots. *Adv Mater* 2024; **36**: 2312313.

70 Ahn C, Li K, Cai S. Light or Thermally powered autonomous rolling of an elastomer rod. *ACS Appl Mater Interfaces* 2018; **10**: 25689–25696.

71 Zhao Y, Hong Y, Li Y, *et al.* Physically intelligent autonomous soft robotic maze escaper. *Sci Adv* 2023; **9**: eadi3254.

72 Zhao Y, Chi Y, Hong Y, *et al.* Twisting for soft intelligent autonomous robot in unstructured environments. *Proc Natl Acad Sci USA* 2022; **119**: e2200265119.

73 Kotikian A, McMahan C, Davidson EC, *et al.* Untethered soft robotic matter with passive control of shape morphing and propulsion. *Sci Robot* 2019; **4**: eaax7044.

74 Liu C, Li K, Yu X, *et al.* A multimodal self-propelling tensegrity structure. *Adv Mater* 2024; **36**: 2314093.

75 Pang W, Xu S, Wu J, *et al.* A soft microrobot with highly deformable 3D actuators for climbing and transitioning complex surfaces. *Proc Natl Acad Sci USA* 2022; **119**: e2079939177.

76 Wu S, Hong Y, Zhao Y, *et al.* Caterpillar-inspired soft crawling robot with distributed programmable thermal actuation. *Sci Adv* 2023; **9**: eadf8014.

77 Zhang H, Yang X, Valenzuela C, *et al.* Wireless power transfer to electrothermal liquid crystal elastomer actuators. *ACS Appl Mater Interfaces* 2023; **15**: 27195–27205.

78 Boothby JM, Gagnon JC, McDowell E, *et al.* An untethered soft robot based on liquid crystal elastomers. *Soft Robot* 2022; **9**: 154–162.

79 Zhao L, Tian H, Liu H, *et al.* Bio-inspired soft-rigid hybrid smart artificial muscle based on liquid crystal elastomer and helical metal wire. *Small* 2023; **19**: 2206342.

80 Min J, Wu Z, Zhang W, *et al.* Intelligent liquid crystal elastomer actuators with high mechanical strength, self-sensing, and automatic control. *Adv Sensor Res* 2023; **3**: 2300117.

81 Wang C, Sim K, Chen J, *et al.* Soft ultrathin electronics innervated adaptive fully soft robots. *Adv Mater* 2018; **30**: 1706695.

82 Ford MJ, Ambulo CP, Kent TA, *et al.* A multifunctional shape-morphing elastomer with liquid metal inclusions. *P Natl Acad Sci* 2019; **116**: 21438–21444.

83 Kotikian A, Morales JM, Lu A, *et al.* Innervated, self-sensing liquid crystal elastomer actuators with closed loop control. *Adv Mater* 2021; **33**: 2101814.

84 Chen G, Ma B, Chen Y, *et al.* Soft robots with plant-inspired gravitropism based on fluidic liquid metal. *Adv Sci* 2024; **11**: 2306129.

85 He Q, Wang Z, Wang Y, *et al.* Electrically controlled liquid crystal elastomer-based soft tubular actuator with multimodal actuation. *Sci Adv* 2019; **5**: eaax5746.

86 Wang Z, Li K, He Q, *et al.* A light-powered ultralight tensegrity robot with high deformability and load capacity. *Adv Mater* 2019; **31**: 1806849.

87 Kim H, Lee JA, Ambulo CP, *et al.* Intelligently actuating liquid crystal elastomer-carbon nanotube composites. *Adv Funct Mater* 2019; **29**: 1905063.

88 Liu J, Gao Y, Wang H, *et al.* Shaping and locomotion of soft robots using filament actuators made from liquid crystal elastomer-carbon nanotube composites. *Adv Intell Syst* 2020; **2**: 1900163.

89 Wang Y, Dang A, Zhang Z, *et al.* Repeatable and reprogrammable shape morphing from photoresponsive gold nanorod/liquid crystal elastomers. *Adv Mater* 2020; **32**: 2004270.

90 Kuenstler AS, Chen Y, Bui P, *et al.* Blueprinting photothermal shape-morphing of liquid crystal elastomers. *Adv Mater* 2020; **32**: 2000609.

91 Song C, Zhang Y, Bao J, *et al.* Light-responsive programmable shape-memory soft actuator based on liquid crystalline polymer/polyurethane network. *Adv Funct Mater* 2023; **33**: 2213771.

92 Zhang J, Wang Y, Sun Y, *et al.* Multi-stimuli responsive soft actuator with locally controllable and programmable complex shape deformations. *ACS Appl Polym Mater* 2023; **5**: 6199–6211.

93 Liang Z, Jin B, Zhao H, *et al.* Rotini-like MXene@LCE actuator with diverse and programmable actuation based on dual-mode synergy. *Small* 2024; **20**: 2305371.

94 Zhang Y, Song C, Bao J, *et al.* Near-infrared light-driven liquid crystalline elastomers with simultaneously enhanced actuation strain and stress. *Sci China Mater* 2023; **66**: 4803–4813.

95 Hu J, Nie Z, Wang M, *et al.* Springtail-inspired light-driven soft jumping robots based on liquid crystal elastomers with monolithic three-leaf panel fold structure. *Angew Chem Int Ed* 2023; **135**: 202218227.

96 Yang M, Xu Y, Zhang X, *et al.* Bioinspired phototropic MXene-reinforced soft tubular actuators for omnidirectional light-tracking and adaptive photovoltaics. *Adv Funct Mater* 2022; **32**: 2201884.

97 Yang Y, Meng L, Zhang J, *et al.* Near-infrared light-driven MXene/liquid crystal elastomer bimorph membranes for closed-loop controlled self-sensing bionic robots. *Adv Sci* 2024; **11**: 2307862.

98 Zhao Y, Li Q, Liu Z, *et al.* Sunlight-powered self-excited oscillators for sustainable autonomous soft robotics. *Sci Robot* 2023; **8**: eadf4753.

99 Mohr R, Kratz K, Weigel T *et al.* Initiation of shape-memory effect by inductive heating of magnetic nanoparticles in thermoplastic polymers. *P Natl Acad Sci* 2006; **103**: 3540–3545.

100 Noh S, Moon SH, Shin T *et al.* Recent advances of magneto-thermal capabilities of nanoparticles: From design principles to biomedical applications. *Nano Today* 2017; **13**: 61–76.

101 Wang Y, Liu J, Yang S. Multi-functional liquid crystal elastomer composites. *Appl Phys Rev* 2022; **9**: 011301

102 Wu Y, Zhang S, Yang Y *et al.* Locally controllable magnetic soft actuators with reprogrammable contraction-derived motions. *Sci Adv* 2022; **8**: eabo6021.

103 Mirvakili SM, Hunter IW. Artificial muscles: mechanisms, applications, and challenges. *Adv Mater* 2018; **30**: 1704407.

104 Naciri J, Srinivasan A, Jeon H, *et al.* Nematic elastomer fiber actuator. *Macromolecules* 2003; **36**: 8499–8505.

105 Fleischmann EK, Forst FR, Zentel R. Liquid-crystalline elastomer fibers prepared in a microfluidic device. *Macromol Chem Phys* 2014; **215**: 1004–1011.

106 Tian X, Guo Y, Zhang J, *et al.* Fiber actuators based on reversible thermal responsive liquid crystal elastomer. *Small* 2024; **20**: 2306952.

107 Xue J, Wu T, Dai Y, *et al.* Electrospinning and electrospun nanofibers: methods, materials, and applications. *Chem Rev* 2019; **119**: 5298–5415.

108 Wu D, Li X, Zhang Y, *et al.* Novel biomimetic "spider web" robust, super-contractile liquid crystal elastomer active yarn soft actuator. *Adv Sci* 2024; **11**: 2400557.

109 He Q, Wang Z, Wang Y, *et al.* Electrospun liquid crystal elastomer microfiber actuator. *Sci Robot* 2021; **6**: eabi9704.

110 Shang L, Yu Y, Liu Y, *et al.* Spinning and applications of bioinspired fiber systems. *ACS Nano* 2019; **13**: 2749–2772.

111 Wu D, Zhang Y, Yang H, *et al.* Scalable functionalized liquid crystal elastomer fiber soft actuators with multi-stimulus responses and photoelectric conversion. *Mater Horiz* 2023; **10**: 2587–2598.

112 Hou W, Wang J, Lv JA. Bioinspired liquid crystalline spinning enables scalable fabrication of high-performing fibrous artificial muscles. *Adv Mater* 2023; **35**: 2211800.

113 Wang Q, Tian X, Zhang D, *et al.* Programmable spatial deformation by controllable off-center freestanding 4D printing of continuous fiber reinforced liquid crystal elastomer composites. *Nat Commun* 2023; **14**: 3869.

114 Lugger SJD, Engels TAP, Cardinaels R, *et al.* Melt-extruded thermoplastic liquid crystal elastomer rotating fiber actuators. *Adv Funct Mater* 2023; **33**: 2306853 .

115 Lin X, Saed MO, Terentjev EM. Continuous spinning aligned liquid crystal elastomer fibers with a 3D printer setup. *Soft Matter* 2021; **17**: 5436–5443.

116 Roach DJ, Yuan C, Kuang X, *et al.* Long liquid crystal elastomer fibers with large reversible actuation strains for smart

textiles and artificial muscles. *ACS Appl Mater Interfaces* 2019; **11**: 19514–19521.

117 Sun J, Wang Y, Liao W, *et al.* Ultrafast, high-contractile electrothermal-driven liquid crystal elastomer fibers towards artificial muscles. *Small* 2021; **17**: 2103700.

118 Mieszczanek P, Robinson TM, Dalton PD, *et al.* Convergence of machine vision and melt electrowriting. *Adv Mater* 2021; **33**: 2100519.

119 Brown TD, Dalton PD, Hutmacher DW. Melt electrospinning today: An opportune time for an emerging polymer process. *Prog Polym Sci* 2016; **56**: 116–166.

120 Javadzadeh M, Del Barrio J, Sánchez Somolinos C. Melt electrowriting of liquid crystal elastomer scaffolds with programmed mechanical response. *Adv Mater* 2023; **35**: 2209244.

121 Feng X, Wang L, Xue Z, *et al.* Melt electrowriting enabled 3D liquid crystal elastomer structures for cross-scale actuators and temperature field sensors. *Sci Adv* 2024; **10**: eadk3854.

122 Wang Y, He Q, Wang Z, *et al.* Liquid crystal elastomer based dexterous artificial motor unit. *Adv Mater* 2023; **35**: 2211283.

123 He Q, Wang Z, Song Z, *et al.* Bioinspired design of vascular artificial muscle. *Adv Mater Technol* 2019; **4**: 1800244.

124 He Q, Wang Z, Wang Y, *et al.* Recyclable and self-repairable fluid-driven liquid crystal elastomer actuator. *Acs Appl Mater Interfaces* 2020; **12**: 35464–35474.

125 Zadan M, Patel DK, Sabelhaus AP, *et al.* Liquid crystal elastomer with integrated soft thermoelectrics for shape memory actuation and energy harvesting. *Adv Mater* 2022; **34**: 2200857.

126 Chi Y, Li Y, Zhao Y, *et al.* Bistable and multistable actuators for soft robots: structures, materials, and functionalities. *Adv Mater* 2022; **34**: 2110384.

127 Hebner TS, Korner K, Bowman CN, *et al.* Leaping liquid crystal elastomers. *Sci Adv* 2023; **9**: eade1320.

128 Jeon J, Choi J, Lee H, *et al.* Continuous and programmable photomechanical jumping of polymer monoliths. *Mater Today* 2021; **49**: 97–106.

129 Annapooranan R, Wang Y, Cai S. Harnessing soft elasticity of liquid crystal elastomers to achieve low voltage driven actuation. *Adv Mater Technol* 2023; **8**: 2201969.

130 Fowler HE, Rothemund P, Keplinger C, *et al.* Liquid crystal elastomers with enhanced directional actuation to electric fields. *Adv Mater* 2021; **33**: 2103806.

131 Davidson ZS, Shahsavan H, Aghakhani A, *et al.* Monolithic shape-programmable dielectric liquid crystal elastomer actuators. *Sci Adv* 2019; **5**: eaay0855.

132 Zhang C, Chen G, Zhang K, *et al.* Repeatedly programmable liquid crystal dielectric elastomer with multimodal actuation. *Adv Mater* 2024; **36**: 2313078.

133 Silva PES, Lin X, Vaara M, *et al.* Active textile fabrics from weaving liquid crystalline elastomer filaments. *Adv Mater* 2023; **35**: 2210689.

134 Sun J, Liao W, Yang Z. Additive manufacturing of liquid crystal elastomer actuators based on knitting technology. *Adv Mater* 2023; **35**: 2302706.

Figures and tables

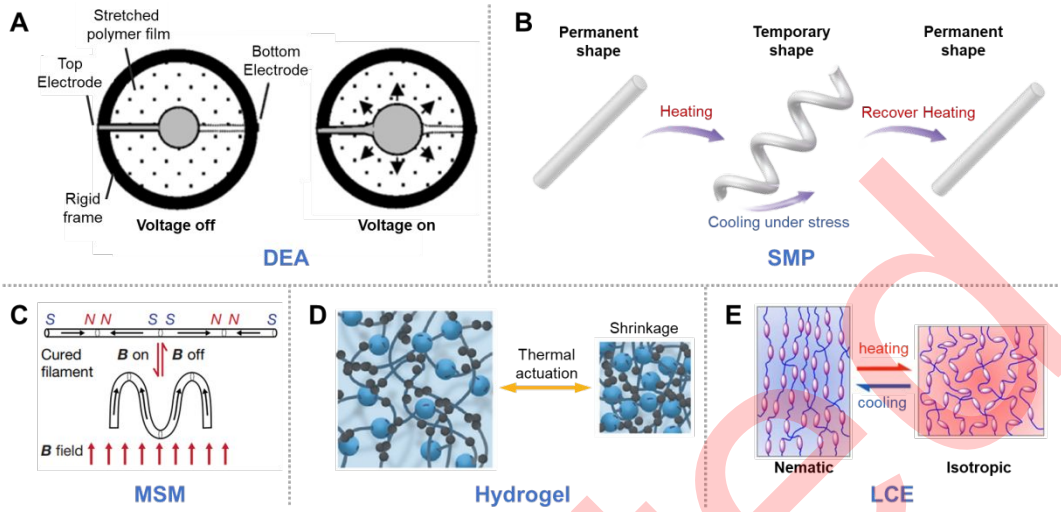

Figure 1 The actuation mechanism of typical soft actuating materials. (A) When subject to high voltage, a strong electrostatic interaction is generated between two electrodes, compressing the film in the thickness direction and expanding it in the area. Reprinted with permission from Ref [6]. (B) After being deformed at high temperature and fixed into a temporary shape after cooling, shape memory polymer (SMP) can recover to its permanent shape upon heating. Reprinted with permission from Ref [9]. (C) Magnetic soft material (MSM) with programmed magnetic domains exhibits complex shape changes under external magnetic field stimulus. Reprinted with permission from Ref [10]. (D) Thermal stimulated isotropic volumetric change of poly (N-isopropylacrylamide) (PNIPAAm) hydrogel. Reprinted with permission from Ref [14]. (E) Upon thermal stimuli, LCE undergoes the nematic-isotropic phase transition, causing a large contraction in the alignment direction. Reprinted with permission from Ref [57].

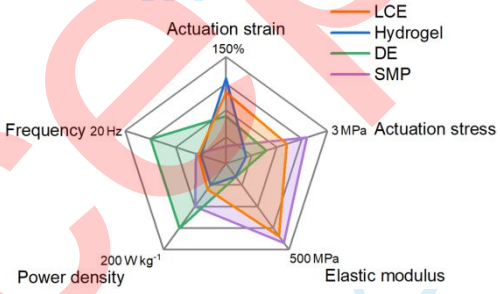

Figure 2 Actuation performances of different soft actuating materials.

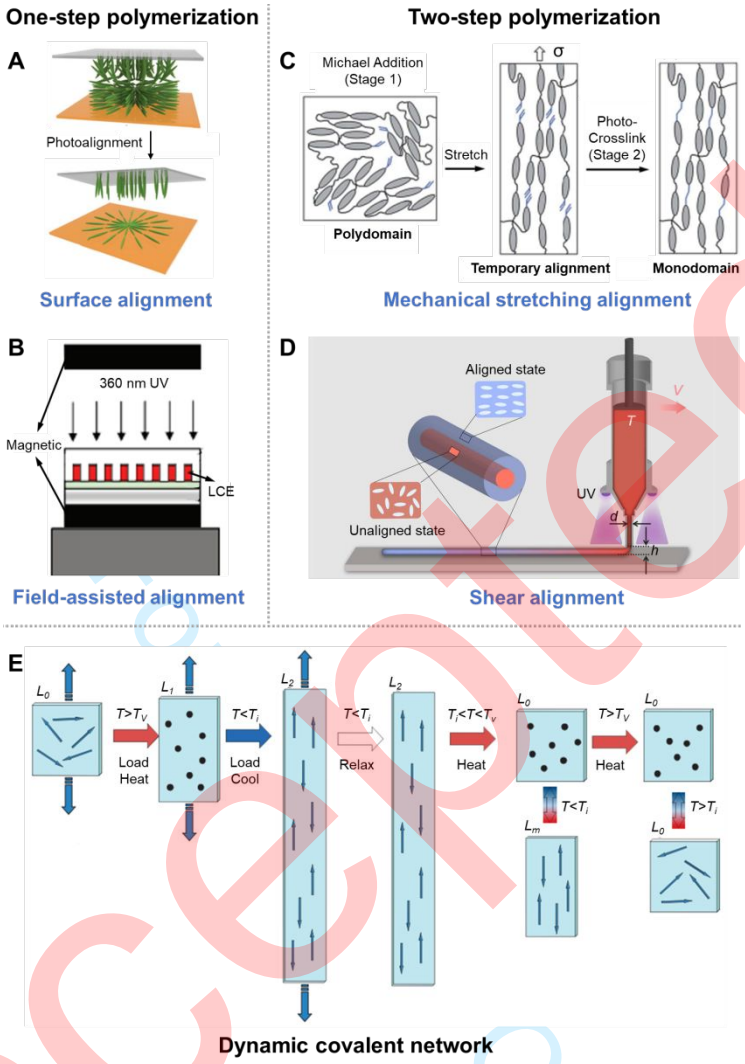

Figure 3 Synthesis and alignment of LCEs. (A) In the one-polymerization method with surface alignment technique, liquid crystal monomer mixture adopts a centrally symmetric splayed alignment directed by molecular orientation at the top and bottom surfaces. Reprinted with permission from Ref [32]. (B) The mesogens align along the longitudinal axis of the LCE pillars by the application of a magnetic field. Reprinted with permission from Ref [34]. (C) The process of a typical two-step polymerization method. The thiol-acrylate Michael addition and photopolymerization (TAMAP) reactions are used to synthesize monodomain LCEs. The polydomain LCE is prepared first and mechanically stretched to align the mesogens into a temporary monodomain. Then, the alignment is fixed through the second-step crosslinking process. Reprinted with permission from Ref [36]. (D) Schematic illustration of the DIW of LCE. The mesogens are aligned along the printing path by shear stress and then are fixed by post-curing. Reprinted with permission from Ref [47]. (E) The schematic illustration of preparing monodomain with dynamic covalent chemistry method. First, the polydomain LCE is uniaxial stretched under external forces and the exchange reaction of dynamic bonds is activated under external stimuli, leading to the rearrangement of the polymer network. As a result, the LCE is programmed into a monodomain state. Reprinted with permission from Ref [48].

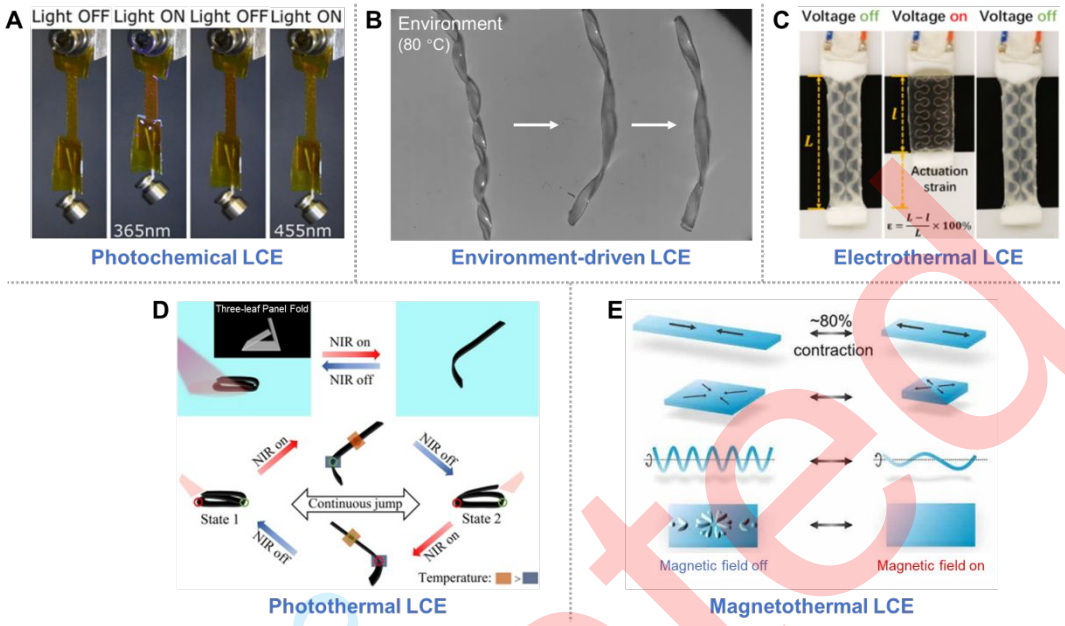

Figure 4 Actuation performance of LCEs with different actuation types. (A) Photochemical mechanism. Under UV irradiation, azobenzene molecules can transition from trans to cis isomerization, leading to the contraction of the LCE strip. After exposure to blue light (455 nm), the LCE strip returns to its original shape. Reprinted with permission from Ref [67]. (B) Environmental heat mechanism. A helical-shaped LCE self-rolling robot powered by environmental heat achieves autonomous locomotion. Reprinted with permission from Ref [72]. (C) Electro-thermal mechanism. Joule heat is generated when a voltage is applied to the metallic wire, increasing the temperature and causing LCE to contract in the longitudinal direction. After turning off the voltage, the LCE gradually recovers to its original shape. Reprinted with permission from Ref [85]. (D) Photo-thermal mechanism. When the CNT-LCE ribbon is exposed to NIR light, CNT can convert the light to heat, causing the temperature to increase and further inducing the deformation. Reprinted with permission from Ref [95]. (E) Magneto-thermal mechanism. The Fe_3O_4 nanoparticle doped-LCE actuators can exhibit different motion modes under the alternating magnetic fields. Reprinted with permission from Ref [102].

Table 1 The actuation performance of conventional LCEs and human skeleton muscle regarding actuation strain, stress, response time (actuation and recovery), work density, and power density

Materials	Actuation strain (%)	Actuation stress (MPa)	Actuation time (s)	Recovery time (s)	Work density (kJ m^{-3})	Power density (W kg^{-1})	References
Environment-driven LCE	44	0.19	180	210	40	0.21	40
CNT-LCE	15	1.02	42	50	38	1.66	88
Heating wire-LCE	41	0.35	30	240	150	0.53	85
Heating wire-LCE	28	0.23	23	180	80	0.32	78
Heating wire-LCE	32	0.49	20	150	340	0.58	59
Heating wire-LCE	40	0.44	30	100	110	1.35	79
LM-LCE	50	0.15	15	125	180	0.54	82
Human muscle	50	0.35	—	—	40	50	103

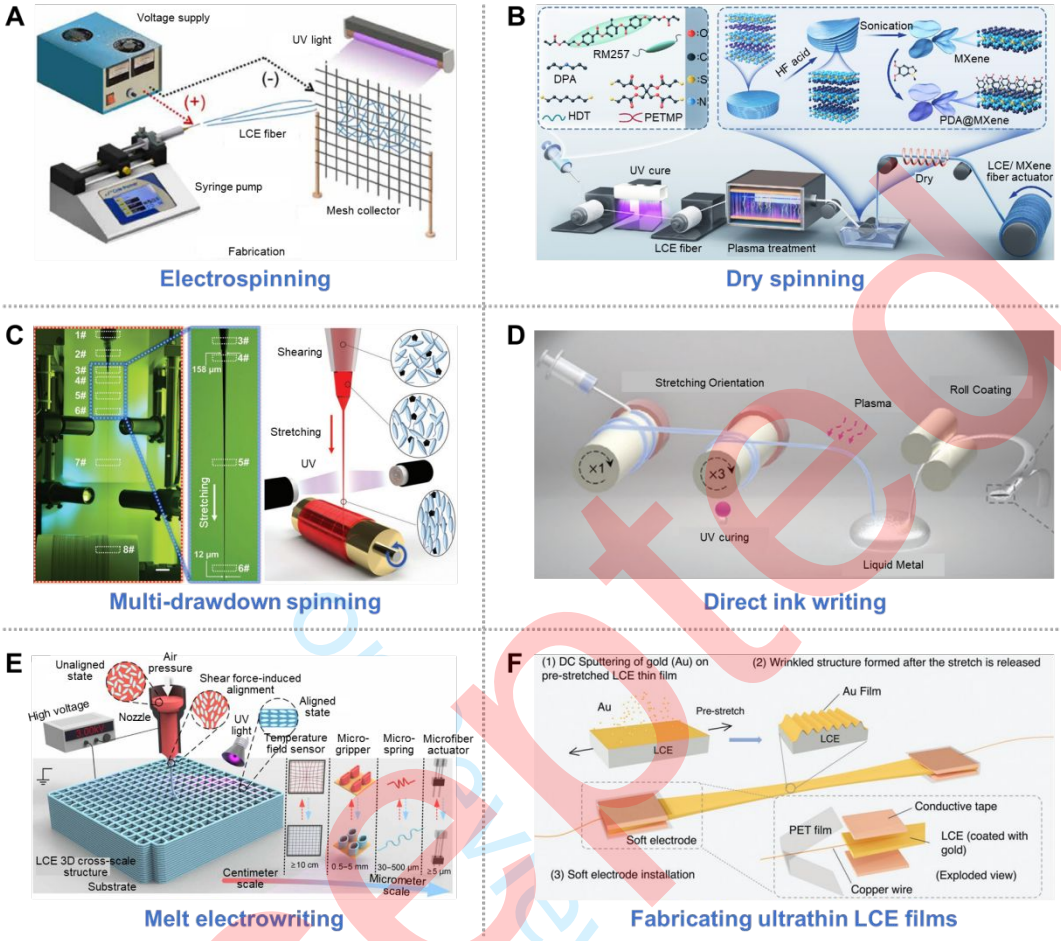

Figure 5 Different strategies to reduce the critical length scale of LCEs. (A) Schematic of the electrospinning of LCE microfiber. Reprinted with permission from Ref [109]. (B) Schematic illustration of the preparation process of the PDA-modified MXene/LCE fiber by dry spinning. Reprinted with permission from Ref [111]. (C) Schematic of fiber shaping and orientation using the multi-drawdown spinning technique. Reprinted with permission from Ref [112]. (D) Schematic diagram of the preparation of LM-LCE fiber via DIW printing. Reprinted with permission from Ref [117]. (E) Schematic illustration of 3D MEW-printed LCE microfibers and cross-scale structures. Reprinted with permission from Ref [121]. (F) Schematic of fabricating ultrathin gold-film-coated LCE film. Reprinted with permission from Ref [122].

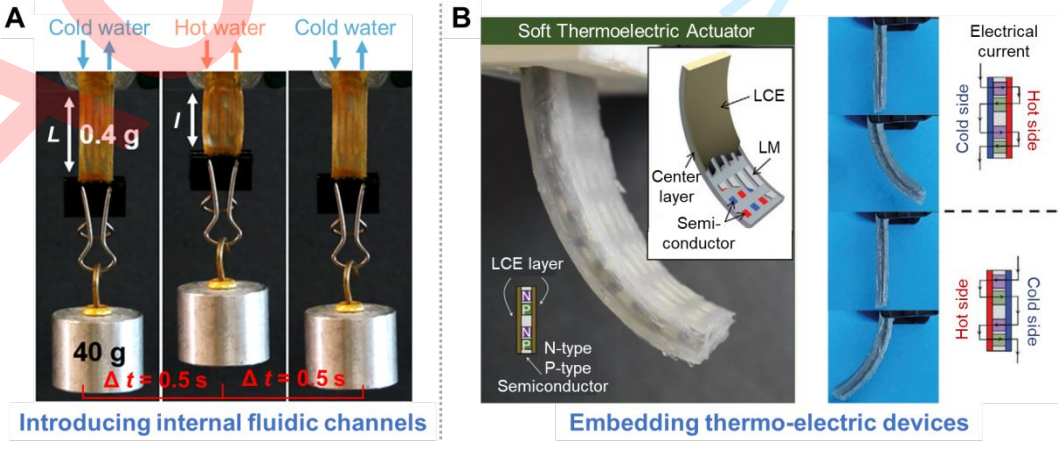

Figure 6 Internal and active heating and cooling systems in LCEs. (A) Introducing the microfluidic channel. The LCE actuator containing a microfluidic channel can produce fast actuation and recovery by alternately injecting hot water (90°C) and cold water (20°C). Reprinted with permission from Ref [124]. (B) Integrating thermal electric device. When a current is applied to a soft TED, the right side of the LCE contracts due to the heating by the Peltier effect, causing the TED-LCE to bend uniformly in the counterclockwise direction. Reversing the flow of current causes the right side that was previously heating to subsequently actively cool and the left side of the device to heat up, resulting in bending in the clockwise direction. Reprinted with permission from Ref [125].

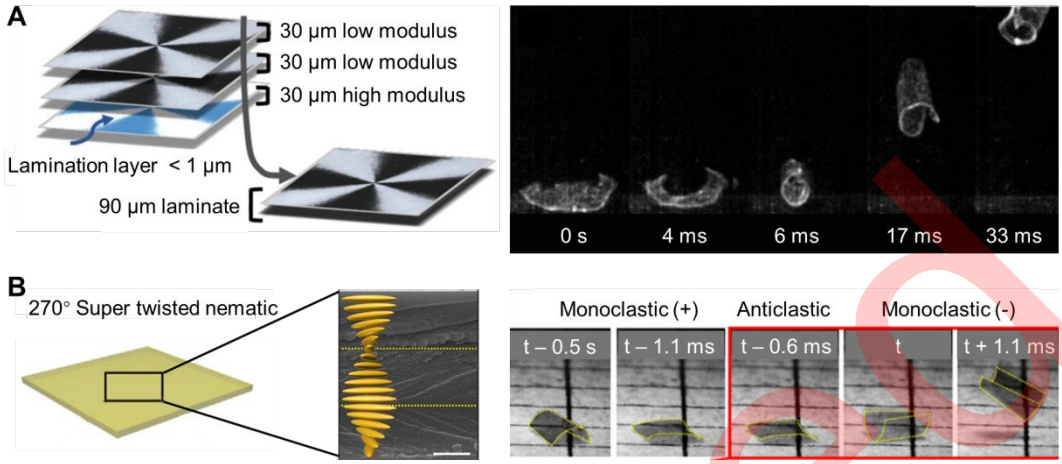

Figure 7 Utilizing mechanical instability of LCEs to achieve rapid actuation. (A) An LCE film is prepared by stacking patterned LCEs to create a modulus gradient through the thickness. Upon heating, the laminated LCE jumps from the hot surface due to a snap-through instability. Reprinted with permission from Ref [127]. (B) An LCN monolith with 270° super twisted nematic alignment of mesogens undergoes mechanical snap-through instability, resulting in the jumping motion. Reprinted with permission from Ref [128].

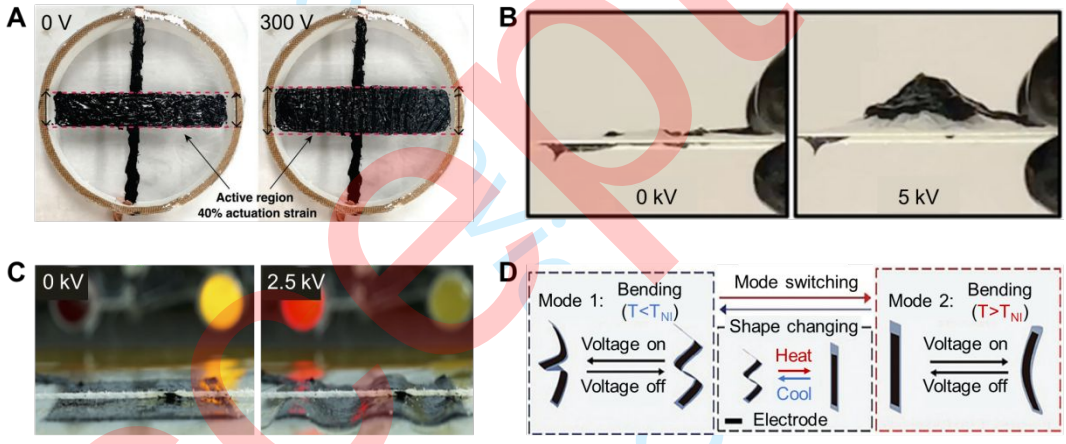

Figure 8 Developing dielectric liquid crystal elastomers. (A) The dielectric LCE film achieves fast and large actuation at a low voltage. Reprinted with permission from Ref [129]. (B) A flat DLCE film exhibits a three-dimensional cone deformation under Maxwell stress when a voltage is applied. Reprinted with permission from Ref [130]. (C) A DLCE device generates 2D to 3D shape change with nonlocal Gaussian curvature at a voltage of 2.5 kV. Reprinted with permission from Ref [131]. (D) The actuation mode switching of DLCE is based on the reversible LCE shape-changing. Reprinted with permission from Ref [132].

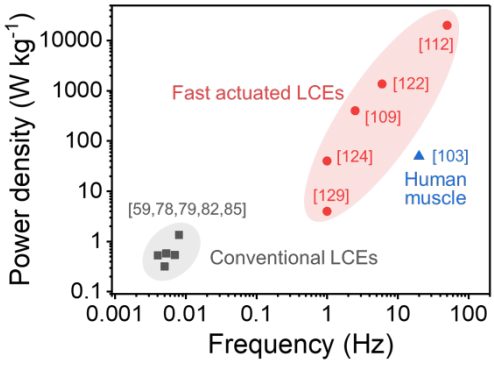

Figure 9 Comparison of frequency and power density between traditional and fast-actuated LCEs. By adopting the strategies mentioned in this paper, the response speed and power density of LCEs have been greatly improved by two orders of magnitude, which are comparable to human skeletal muscle.